Experimental demonstration of ultrahigh-precision transport and acceleration of single ions

K. Muroo,[1,*,‡] K. Hosaka,[2] Y. Yuri,[2] K. Ito,[1] and H. Okamoto[1,†]

[1]*Graduate School of Advanced Science and Engineering, Hiroshima University, 1-3-1 Kagamiyama, Higashi-Hiroshima 739-8530, Japan*

[2]*Takasaki Institute for Advanced Quantum Science, National Institutes for Quantum Science and Technology (QST), 1233 Watanuki, Takasaki, Gunma 370-1292, Japan*

(Received 30 October 2025; accepted 3 April 2026; published 5 May 2026)

A basic performance test of a novel ion source is carried out to attain an extremely narrow beam for pinpoint irradiation of single ions onto an intended target. In principle, the normalized root-mean-squared emittance of the beam can reach a sub-femtometer level, which makes a transverse spot size of nanometer order available. The system is based on a compact linear Paul trap equipped with a Doppler-cooling device. The trap is the most popular, economical type consisting simply of a few metal plates and rods. Among several possible choices of ion species, we picked $^{40}Ca^{+}$ for the present investigation. A small number of $^{40}Ca^{+}$ ions are first laser cooled to near absolute zero where they form a spatially ordered configuration called a *Coulomb crystal*. The axial-potential well provided by dc bias voltages on two planar electrodes is then deformed gradually to eject the ions from the trap along the design orbit. We demonstrate that it is possible to launch the ultracold ions one by one at arbitrary timing with no serious radio-frequency heating. These ions are accelerated to 1 keV immediately after the extraction. The effectiveness of a few different ion-ejection schemes is experimentally verified and supported by three-dimensional molecular dynamics simulations.

DOI: 10.1103/zgph-xm12

I. INTRODUCTION

A variety of charged particle beams have now been employed in diverse fields including fundamental physics, life sciences, industry, radiation therapy, etc. The particle species, kinetic energy, intensity, and other basic parameters of a beam are carefully selected in accordance with the intended use. The focus of the present research is the beam size, or more correctly, how precisely we can control the orbit of a single ion from the source to a target. In some applications of ion beams, the achievable minimum spot size on the target is of essential importance [1–6]. The so-called "microbeam" has been used for such cases to irradiate target materials with very high precision. The transverse size of a microbeam is of a micron or even submicron level, though the intensity is quite low.

A typical procedure for microbeam generation is the combined use of collimators and focusing lenses; we first let a low-current beam go through small apertures and then focus it with electromagnetic elements. This approach is relatively easy to implement, but the achievable emittance is limited depending strongly on the beam transport design and preceding accelerator performance. In the new approach explored below, we carefully manipulate individual ions in a compact source before launching them into the beam transport or accelerating channel that follows. The proposed system can provide an extremely narrow "nanobeam" whose normalized root-mean-squared (rms) emittance is on the order of femtometer or less. In principle, it is possible to control the orbit of a single ion and deliver it to any specific point on an intended target very precisely.

Our novel ion source is based on a linear Paul trap (LPT) that uses radio-frequency (rf) and static electric fields to confine ions three-dimensionally in a tiny space [7]. The stored ions can readily be extracted from the trap by dropping the axial-potential barrier on the exit side, but before extraction, we cool the ion cloud to improve the emittance. This is a striking contrast with conventional microbeam generators where the emittance control is done (e.g., by scraping tail particles off) in the last

*Contact author: muroo.kento@qst.go.jp

†Contact author: okamoto@sci.hiroshima-u.ac.jp

‡Present address: Takasaki Institute for Advanced Quantum Science, National Institutes for Quantum Science and Technology (QST), 1233 Watanuki, Takasaki, Gunma 370-1292, Japan.

Published by the American Physical Society under the terms of the Creative Commons Attribution 4.0 International license. Further distribution of this work must maintain attribution to the author(s) and the published article's title, journal citation, and DOI.

stage *after* the beam reaches a final energy. The LPT is equipped with a Doppler laser cooler that enables us to reduce the cloud temperature close to absolute zero [8,9], which means that the beam emittance is already at the Doppler cooling limit before extraction. We, therefore, need no extra beam-manipulator system for emittance improvement, unless serious beam heating occurs during the extraction process.

The idea of using a compact LPT as an ultralow-emittance ion source was first discussed in Refs. [10,11]. Later, a few research groups actually constructed LPT-based ion sources from which ultracold $^{40}Ca^{+}$ ions were ejected along the LPT axis with no rf heating [12,13]. A European research team even succeeded in extracting *sympathetically* cooled ions for the creation of nitrogen-vacancy centers in diamond, as a promising platform of some future quantum technologies [14].

We here report on the results of further experimental tests, trying a few different ion-extraction schemes. We demonstrate experimentally and numerically for the first time that it is possible to launch ultracold ions one by one from the LPT at arbitrary timing, simply by manipulating the dc potential of a specific electrode. The use of a two-dimensional type of crystalline structure, never considered in any previous studies on this theme, is also explored experimentally and shown to work for the present purpose. A brief description of our experimental system is offered in Sec. II. It is not necessary to design an elaborate trap; a very simple four-rod LPT, the most standard type widely used for a variety of applications, suffices for nanobeam generation [13]. Three-dimensional (3D) numerical simulation data are then given in Sec. III for comparison with experimental observations summarized in Sec. IV. Concluding remarks are finally made in Sec. V.

II. EXPERIMENTAL SYSTEM

The LPT employed for the present experiment was constructed recently at the Takasaki Institute for Advanced Quantum Science. It is one of several main components of the ultrahigh-precision ion implanter designed to supply nanobeams of several different ion species such as Ca, N, and Si [15]. In addition to the LPT section sketched in Fig. 1, the novel implanter also includes a primary liquid-metal ion source (LMIS) [16], laser systems for the ionization and Doppler cooling of Ca, and an electrostatic bipotential-lens section where a nanobeam from the LPT can be accelerated up to 50 keV for singly charged ions. Charged particles from the gallium LMIS are selected, before reaching the LPT, in a short transport channel with a Wien filter, a quadrupole bender, and Einzel lenses. The laser ionization method is applied to produce $^{40}Ca^{+}$ ions from neutral Ca atoms provided by a compact dispenser. Those $^{40}Ca^{+}$ ions trapped in the LPT are Doppler cooled with two lasers that have the wavelengths of 397 and 866 nm; the former laser is for the cooling transition ($4s^2S_{1/2} \leftrightarrow 4p^2P_{1/2}$) and the latter for repumping ions in the metastable state ($3d^2D_{3/2}$) back to the upper level ($4p^2P_{1/2}$).

The mechanical design of the LPT is similar to the one developed for the first "ion machine-gun" experiment at Hiroshima University [13]. The operating frequency was set at 1.94 MHz, slightly lower than the previous experiment (performed at 2 MHz). The minimum distance from the LPT axis to the quadrupole rods is 3.0 mm. These rods have a diameter (6.88 mmϕ) somewhat larger than the

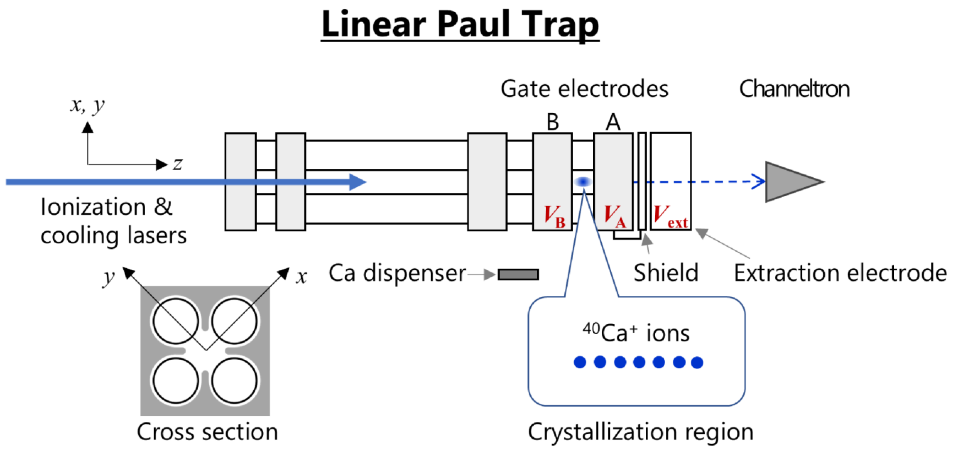


FIG. 1. Layout of the experiment. The LPT has a simple *four-rod* structure [7] with five planar electrodes (shaded). All these electrodes are electrically isolated so that we can apply different rf and/or dc voltages to them. The aperture size is 6 mm in diameter. In the present study, $^{40}Ca^{+}$ ions are stored and laser cooled in the region between the two planar electrodes named "Gate A" and "Gate B." Axial confinement of ions is achieved by dc voltages (V_A and V_B) added to these Gate electrodes. Another planar electrode, which has a high potential of V_{ext} for ion acceleration, is placed 5 mm away from Gate A. Extracted ions are detected by a channel electron multiplier (channeltron) sitting 59 mm away from the LPT exit. Lasers for Doppler cooling and for ionization of neutral Ca atoms from a compact dispenser are introduced along the LPT axis.

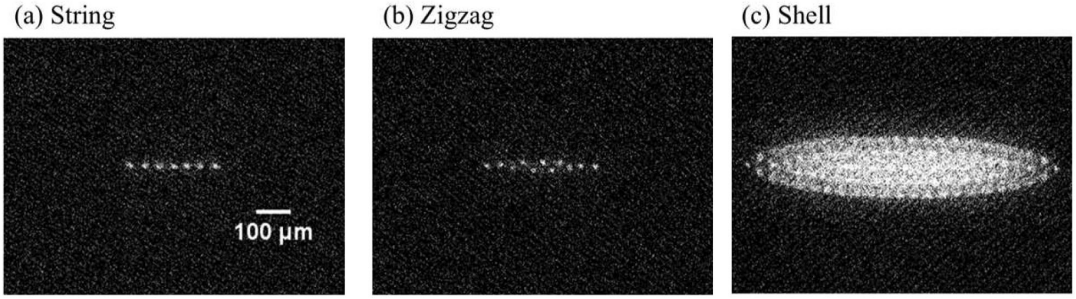


FIG. 2. Coulomb crystals. Each bright dot corresponds to a single $^{40}Ca^{+}$ ion laser cooled in the LPT. These three crystalline structures are referred to as (a) string, (b) zigzag, and (c) shell. The structural transition occurs depending on the line density and the strength of the external focusing force [20].

aperture size (6.0 mmϕ) to minimize the nonlinear multipole fields inevitably excited due to their circular surface; the boundary must be hyperbolic to create a pure quadrupole field in the aperture [17,18]. The amplitude of the rf quadrupole potential for transverse ion confinement is typically adjusted to 24 V. This corresponds to a betatron phase advance of 22° per rf period when the Gate electrodes in Fig. 1 have the potential of 0.3 V.

An rf quadrupole field is used to confine ions in the transverse degrees of freedom. The axial confinement of ions can be done with low dc voltages applied to planar electrodes electrically isolated from the quadrupole rods. Five plates (shaded in Fig. 1) are aligned so that we can provide a few potential wells along the z axis, if necessary. The heights of the dc barriers are carefully controlled to capture hot ions of a specific species from the Ga LMIS, eventually laser cooled directly or sympathetically to near absolute zero. The overall length of the LPT section is 177.5 mm. The quadrupole rods are separated into two parts near the center so that the two sections can have different base potential levels. For the present purpose, however, no complicated control of the axial-potential shape is demanded as we only need $^{40}Ca^{+}$ ions from the dispenser. All we have to do is add low voltages V_A and V_B to the two Gates as illustrated in Fig. 1; $^{40}Ca^{+}$ ions are stored within a limited region between Gate A and Gate B near the exit end. These Gates are spaced 6 mm apart; the distance is equal to the aperture size, which makes the axial potential well roughly parabolic when $V_A = V_B$.

Of primary importance at this stage is to accumulate know-how on various extraction schemes of ultracold ions, so we did not activate the bipotential lens. Instead, an extraction electrode right after the LPT was biased to V_{ext} to accelerate ions toward a channel electron multiplier (CEM). We have chosen V_{ext} to be -1 kV so far. A shield plate, which has the same potential as Gate A, must then be inserted between Gate A and the extraction electrode to avoid the distortion of the ion confinement potential in the LPT. The CEM is placed 59 mm away from the LPT exit to detect the signal of each individual ion. The base vacuum pressure in the chamber is about 2.0×10^{-8} Pa.

After laser cooling to near the Doppler limit, i.e., 0.5 mK for $^{40}Ca^{+}$, the ultracold ion cloud establishes a spatially ordered configuration called a *Coulomb crystal* [19,20]. In a crystalline state, the Coulomb repulsion between individual ions balances with the external focusing force provided by the rf and dc potentials of the electrodes. A few examples of laser-induced fluorescence (LIF) images from Coulomb crystals detected by a charge-coupled device (CCD) camera are displayed in Fig. 2. At low line density, the crystalline structure is the so-called *string* where all ions are aligned along the LPT axis at almost equal intervals. Increasing the number of stored ions, we can convert the string into the *zigzag* and eventually into the *shell* configuration.

A crystal of the string type is preferable for the following experiment as we can most easily separate one ion from the others. The initial number of ions (N_{in}) should thus be small though the precise control of N_{in} is difficult in practice. At the very beginning, we often obtain an ellipsoidal crystal that has a few shells as in Fig. 2(c). We can, however, reduce N_{in} by giving quick distortion to the axial potential shape; for instance, V_B on Gate B is raised to a specific value and quickly back to the original voltage. According to our past experience, just one up-down switch in V_B allows us to start the experiment with a proper N_{in} at which the resultant crystalline structure is the string type. In a typical case where the initial Gate potential is set at 0.3 V, V_B is usually increased to around 8.0 V in 10 ms, maintained there for 5 ms, and finally reduced to the original voltage in 10 ms. This procedure is similar to what we take for the slow extraction discussed in Sec. IV B.

III. NUMERICAL TEST

3D multiparticle simulations were carried out to see if it is really possible to separate a single ion from a Coulomb crystal and launch it along the LPT axis without heating. A similar numerical study has been done in Ref. [21] concentrating attention on sympathetically cooled $^{14}N_2^{+}$ ions in a two-component crystal. We developed a molecular dynamics (MD) code in which Coulomb interaction among individual ions can be taken accurately into account. The external electric potential data acquired by

a Maxwell-equation solver (CST Studio Suite [22]) under the boundary condition reflecting the 3D electrode geometry in Fig. 1 are incorporated into the code for reliable simulations. The equations of ion motion are integrated in a symplectic manner, apart from the cooling interaction.

Unlike in the previous simulation study where a simple linear friction model was adopted [21], we here consider the actual Doppler cooling force defined as

$$\boldsymbol{F}_{\mathrm{c}} = \frac{1}{2}\hbar\boldsymbol{k}\Gamma\frac{S}{1+S+[2(\delta-\boldsymbol{k}\cdot\boldsymbol{v})/\Gamma]^2}, \tag{1}$$

where $\hbar\boldsymbol{k}$ is the momentum vector of a laser photon, Γ is the natural line width of the cooling transition, S is the normalized laser intensity, δ is the detuning of the laser frequency from the natural resonant frequency of $^{40}Ca^{+}$, and $\boldsymbol{v}$ is the velocity vector of each individual ion. We assumed a Gaussian laser with the spot size σ, writing $S = S_0\exp(-2(x^2+y^2)/\sigma^2)$ where S_0 is the peak laser intensity normalized by the saturation intensity. A Monte Carlo algorithm was used to introduce the effect of diffusive heating due to the random nature of spontaneous photon emission and absorption. In our experiment discussed in Sec. IV, the cooling laser, injected rightward in Fig. 1, was always on even during the ion extraction process. We, therefore, keep it on in most of the following simulations as well. The total power and spot size are assumed to be 1.6 mW and 0.9 mm (except in the Appendix). These laser parameters, corresponding roughly to the actual experimental conditions, give $S_0 = 2.68$. The detuning ranges from -60 to -24 MHz.

Let us consider a Coulomb crystal consisting of N_{in} ions. It is confined between Gate A and Gate B to which the dc voltages of V_{A} and V_{B} have been applied, respectively. At the beginning, we set $V_{\mathrm{A}} = V_{\mathrm{B}}(\equiv V_{\mathrm{in}})$ to make the axial potential well symmetric about the center of the crystallization region. V_{in} is adjusted to 0.3 V unless otherwise noted.

We have two straightforward ways to push the rightmost ion on the Gate-A side out of the LPT; one way is to increase V_{B}, and the other to decrease V_{A}. Figure 3 shows an example of the former case when $N_{\mathrm{in}} = 5$. V_{B} has been raised linearly from 0.3 to 6.26 V in 10 ms. The final value of V_{B} must be chosen carefully, such that the local minimum of the axial potential does not disappear. Even then, we can eject the rightmost ion from the trap (if the axial potential well is sufficiently shallow) because it is always receiving Coulomb force from all the other ions plus the radiation pressure in the rightward direction. It turns out that the ejection of the single ion happens at $t \approx 10.5$ ms, slightly after V_{B} comes to the final value. A similar delay of ejection timing was observed in the previous simulations with two-component crystals [21]. This is most likely an inertial effect as the ions need some time to respond to the change in the axial potential well. The delay tends to be shortened as we raise V_{B} more quickly. In the case of Fig. 3, only the rightmost ion was launched along the LPT axis and arrived at the detector (located at $z = 79.0$ mm) at $t = 10.535$ ms; the four other ions in Fig. 3(c) stayed in the LPT.

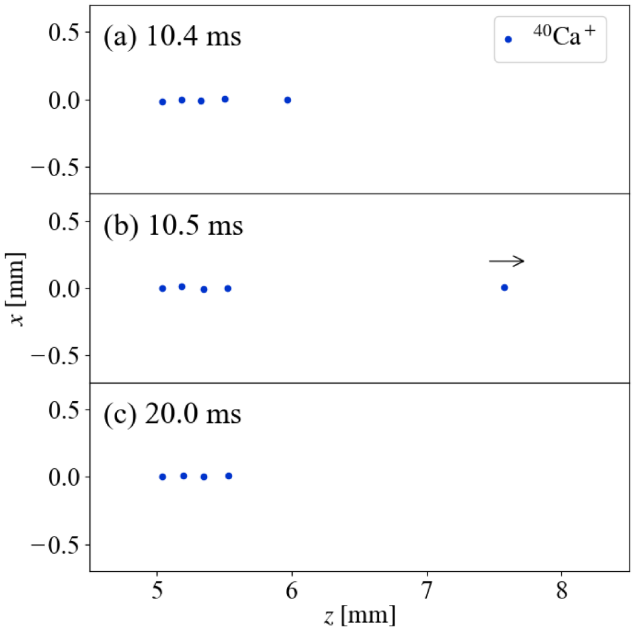


FIG. 3. Single-ion separation from a string Coulomb crystal ($N_{\mathrm{in}} = 5$) by manipulation of the axial ion-confinement potential. Each dot represents one $^{40}Ca^{+}$ ion laser cooled in the LPT. The three panels show the spatial distributions of the ions at (a) 10.4 ms, (b) 10.5 ms, and (c) 20.0 ms after V_{B} starts to vary. The origin of the z coordinate (abscissa) is chosen at the center of the ion confinement region between Gate A and Gate B. Note that the whole crystal has been moved toward the Gate-A side due to the axial-potential distortion caused by the increase of V_{B} on Gate B (and partially to the radiation pressure).

We conducted 100 independent simulations with N_{in} fixed at a specific number, to figure out the expected rms emittance at the detector. 100 different sets of random numbers were used to define the initial coordinates and momenta of individual ions before cooling. The resultant distributions of ions at the detector when $N_{\mathrm{in}} = 5$, corresponding to the case in Fig. 3, are plotted in Fig. 4. In each of these 100 simulations, five $^{40}Ca^{+}$ have been cooled to the Doppler limit, establishing the string formation. Unlike in Fig. 3, we shut down the cooling force once the crystalline state was reached. The final V_{B} for the extraction of the rightmost ion then needs to be slightly increased from 6.26 V in Fig. 3 to 6.33 V here because of the lack of the axial force (radiation pressure) generated during the absorption of many photons. The symbols p_x and p_y stand for the transverse kinetic momenta normalized by mc with m and c being the rest mass of the ion and the speed of light. The transverse normalized rms emittance evaluated from these MD simulations is sub-femtometer level, consistent with the previous numerical study [21].

There is a threshold for the Gate voltage V_{B} above which two or more ions escape from the trap. The final V_{B} needs

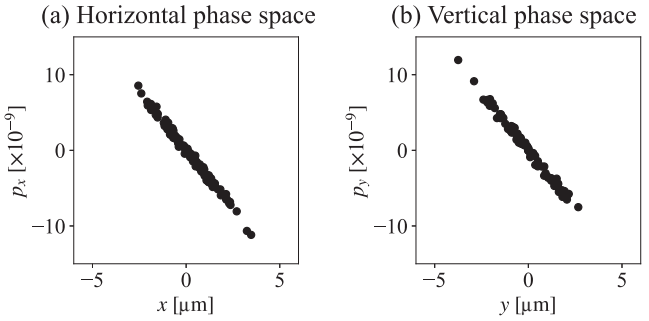


FIG. 4. Transverse phase-space distributions of extracted ions at the CEM detector. A total of 100 independent simulations of single-ion extraction were carried out with N_{in} fixed at 5, starting with ion distributions generated by 100 different sets of random numbers. The operating condition of the LPT is exactly the same as assumed in Fig. 3. The normalized rms emittances in (a) horizontal phase space and (b) vertical phase space are both equal to 4.8×10^{-16} m.

to be slightly below this threshold to ensure the ejection of only a single ion. We expect the threshold value to be higher for a larger V_{in}, in other words, when an axial potential well is initially deeper. This natural expectation is confirmed in Fig. 5 comparing two separate cases where $V_{\mathrm{in}} = 0.3$ and 0.5 V. The reason why the optimum V_{B} decreases with increasing N_{in} is because the interparticle force pushing the rightmost ion toward the LPT exit becomes stronger. The amount of change in the final V_{B} between two adjacent points in Fig. 5 is not equal but becomes smaller gradually with increasing N_{in}. Figure 5 suggests the possibility of launching all N_{in} ions one by one at arbitrary timing by raising the Gate voltage in stages.

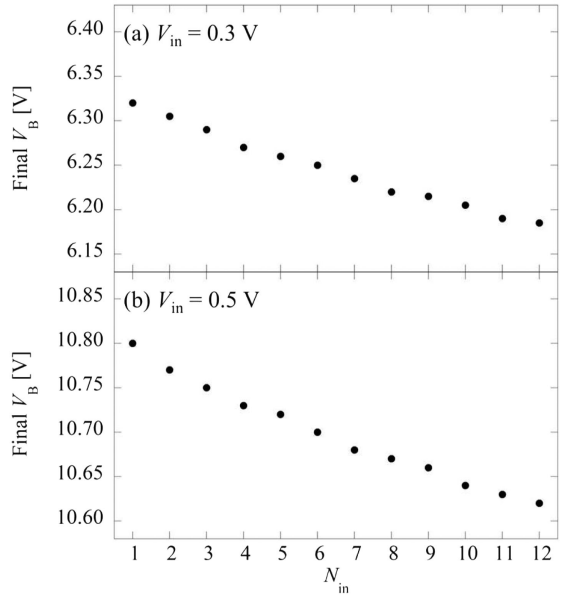


FIG. 5. Final Gate-B voltage required for single-ion ejection. At the beginning, Gate A and Gate B have the same potential: (a) $V_{\mathrm{in}} = 0.3$ V and (b) $V_{\mathrm{in}} = 0.5$ V. We increase the Gate-B voltage V_{B} linearly to a certain final value within 10 ms while keeping the Gate-A voltage at V_{in}. The ordinate indicates the value of V_{B} when only one of the N_{in} ions, positioned at the exit end of the crystal, is ejected from the LPT. The crystalline structure turns from a string to a zigzag configuration at N_{in} greater than 10 in the case (a) and 7 in the case (b). A further structural transition from a zigzag to a shell configuration occurs in the case (b) at $N_{\mathrm{in}} = 11$.

We now control the Gate-A voltage V_{A} instead of V_{B}. The initial voltage of 0.3 V on Gate A is reduced to a certain final value within 3 ms. The final V_{A} required for single-ion ejection is plotted in Fig. 6 as a function of N_{in}. The dependence on N_{in} is attributed to the Coulomb repulsion from the remaining ions, just like the case in Fig. 5. Note that the average increment between two adjacent points in Fig. 6 is only 0.19 mV, much smaller than the decrement of Fig. 5(a) (over 12 mV). This is simply because the depth of the axial potential well is shallower here, compared to the previous case in Fig. 5 where V_{A} (the potential on the exit side) is fixed at V_{in}. The control of V_{A} must thus be performed much more precisely.

The manipulation of the axial potential shape with the electrode voltages is probably the easiest and least complicated way to accomplish our goal. Another possible approach includes the use of the radiation pressure induced by the cooling laser. The Doppler cooling force given by Eq. (1) actually works as numerically demonstrated in the Appendix; it is possible to move a Coulomb crystal toward the LPT exit by sweeping the detuning δ. Choosing proper laser parameters, we can achieve consecutive ejection of ultracold ions from the LPT.

IV. EXPERIMENT

A. Fast extraction

In the proof-of-principle experiment conducted at Hiroshima University [13], we tried to eject a whole string crystal at a time by switching the dc voltages on the two end

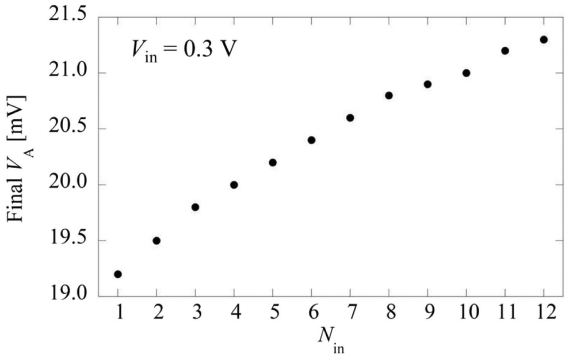


FIG. 6. Final Gate-A voltage required for single-ion ejection. We decrease the Gate-A voltage V_{A} linearly from 0.3 V to a certain final value within 3 ms while keeping the Gate-B voltage at 0.3 V. The ordinate indicates the value of V_{A} when only one of the N_{in} ions, positioned at the exit end of the crystal, is ejected from the LPT.

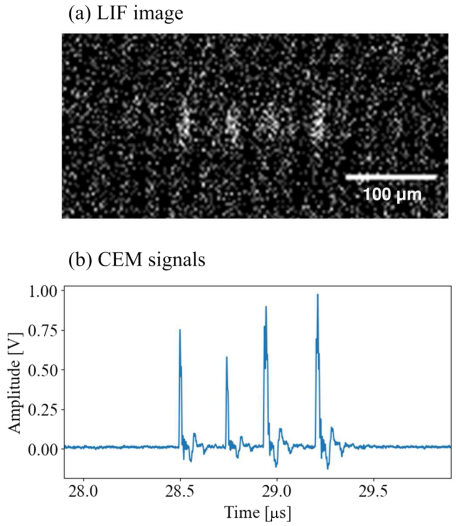


FIG. 7. Fast extraction of a whole string crystal. (a) LIF image of a Coulomb crystal ($N_{in} = 4$) before extraction. (b) Ion signals detected by the CEM. The amplitude of the rf voltage on the quadrupole rods is adjusted to 15.7 V in this experiment. The potential barrier on the Gate-A side was completely removed in 200 ns to eject all four ions from the LPT at a time.

plates simultaneously. The potential barrier on the exit side was simply removed within 10 ns, while the Gate voltage on the other side was increased to 120 V at a maximum to enhance the axial electric field for ion acceleration. The time of flight to the detector actually became shortened as this extraction voltage was made higher. All ion bullets were successfully launched from the LPT and hit the detector at nearly equal time intervals [13].

Before proceeding to the next step, we did a similar experiment on the ion machine-gun concept, using the newly developed LPT system at the Takasaki Institute. Figure 7 offers a typical example where a string crystal consisting of four $^{40}Ca^{+}$ ions is extracted in the same way as mentioned above; specifically, V_A was switched to 0 V in 200 ns, while V_B was changed to 1.3 V. Both Gate electrodes had an identical potential of 0.3 V before the simultaneous switching. Four clear signals from the extracted ions were detected by the CEM around 29 μs after the Gate voltages started to change. The time intervals between neighboring ions are almost equal, which suggests that the string configuration is maintained even after the extraction.

According to systematic MD simulations, the normalized rms emittance of these linearly arranged ions grows during the extraction process when the variation of the axial potential well is too fast. For instance, it was worsened to the order of 10^{-13} m under the experimental condition adopted for the fast-extraction experiment in Ref. [13]. The primary cause of the emittance growth is the interparticle Coulomb collision, in other words, a kind of very weak intrabeam scattering non-negligible at such a low temperature. This type of weak heating mechanism has little effect in the "slow-extraction" scheme explored in the next subsection; the emittance achievable with the new scheme is expected to be 3 orders of magnitudes better. A recent MD study has also concluded that the normalized rms emittance estimated from a series of slow single-ion shots reaches the sub-femtometer range even for nitrogen ions that can only sympathetically be cooled through the Coulomb interaction with calcium ions [21].

B. Slow extraction

We now verify experimentally that the single-ion ejection as numerically studied in Sec. III is feasible. Following the conditions assumed in the MD simulations, we start with the axially symmetric potential well provided by the equal Gate voltages V_{in}. The voltage V_B on Gate B is increased linearly within 10 ms from V_{in} to a certain target value U_B that allows us to eject only the rightmost ion from the LPT. We then reduce V_B back to V_{in} for the sake of visual confirmation of LIF signals from the remaining ions. Ideally, such a return is unnecessary; we may just increase the Gate-B voltage step by step from one target value to the next for consecutive single-ion ejection. This extra step is, however, essential here to make sure that the total number of ions has actually been reduced by one after every ejection procedure. As pointed out in Fig. 3, the increase in V_B causes an asymmetric distortion of the axial potential well, moving the whole crystal to near the LPT exit. All ions are hidden behind the Gate-A electrode as a result, which makes it impossible to detect LIF photons from them. The Gate-B potential must, therefore, be returned to the original value so that we can count the number of remaining ions with the CCD camera.

The left panels in Fig. 8 show the LIF images taken right after every ejection cycle. The string crystal consists of six $^{40}Ca^{+}$ ions at the start. Obviously, we have succeeded in launching them one by one simply by manipulating the Gate potential. In this experiment, V_{in} has been set at 0.3 V. The potential of Gate A is fixed at 0.3 V while the Gate-B voltage goes up and down because of the practical reason explained above. The upper value U_B at each ejection is given in Table I. The Gate-B voltage was maintained at these values for 5 ms and then reduced to 0.3 V in 10 ms for LIF measurement. The holding time of 5 ms can be extended to the order of seconds or even much longer if necessary, which means that we have a very high degree of flexibility in controlling the timing of ion irradiation onto an intended target. In fact, after the completion of each ejection cycle, we usually spend a few tens of seconds for LIF data saving and for manual input of the next U_B to an LPT-control computer.

The ejected ions arrive at the CEM detector around 10.5 ms after V_B starts to increase from 0.3 V, which is in good agreement with the MD simulation in Sec. III. On the other hand, we see only qualitative agreement regarding

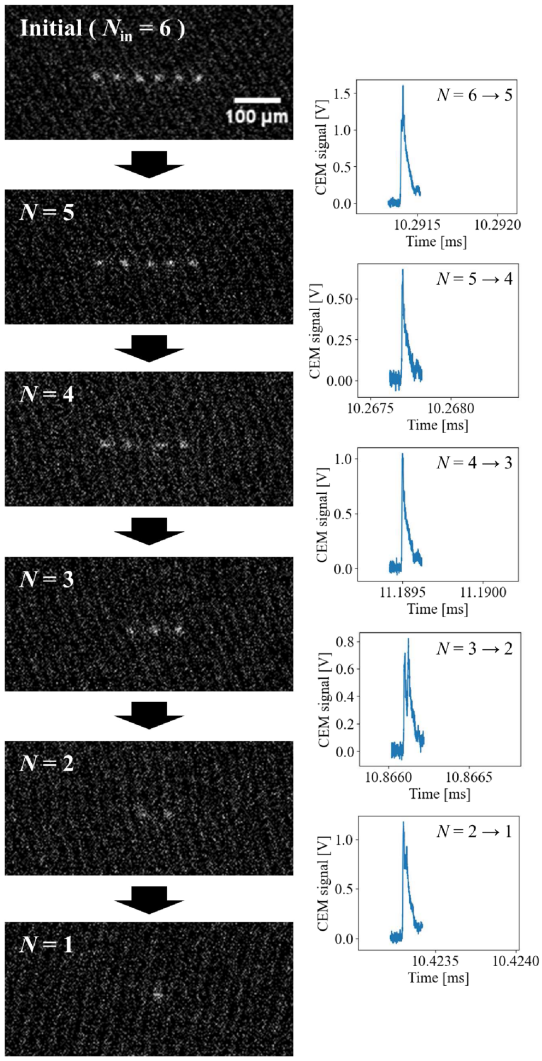


FIG. 8. A sequence of single-ion separation and extraction at $V_{in} = 0.3$ V. The starting crystalline structure is a string consisting of six $^{40}Ca^{+}$ ions ($N_{in} = 6$). These six ions can be ejected one by one from the LPT, as evidenced by the LIF images in the left panels. The right panels show the CEM outputs after every ejection of the rightmost ion. The abscissa is the time measured from each start of V_B ramping from 0.3 V to the extraction voltage U_B in Table I. CEM signals were recorded on a hard disk in the oscilloscope only when their power exceeded the noise level. The time width of each data was limited to 0.2 μs in order to save the disk space.

the extraction threshold U_B. As indicated in Table I, U_B becomes higher for a shorter crystal. It is almost proportional to the number of ions, as in the numerical observation. The absolute value of U_B is, however, roughly 30% greater than the data in Fig. 5(a). The exact reason for this is unknown, but we presently suspect electrode contamination as it produces a kind of contact voltage that affects the actual height of the potential barrier at the exit. Mechanical imperfections such as electrode misalignments could also be a possible cause, though a relatively large amount of error seems necessary to explain the observed discrepancy.

TABLE I. Gate-B voltage U_B used for single-ion ejection experiments in Figs. 8 and 9.

	U_B (V) at single-ion ejection				
Number of ions	6 → 5	5 → 4	4 → 3	3 → 2	2 → 1
$V_{in} = 0.3$ V	8.10	8.14	8.20	8.24	8.28
$V_{in} = 0.5$ V	…	…	…	13.36	13.46

Another sequence of single-ion extraction is shown in Fig. 9 where the axial potential well has been made deeper; V_{in} is 0.5 V here instead of 0.3 V in Fig. 8. N_{in} has been reduced so that we can start with a string configuration for comparison. Similarly to the previous example, V_B is raised from 0.5 V to a specific upper threshold U_B in 10 ms, maintained for 5 ms, and returned to 0.5 V for the observation of LIF photons from the remaining ions. This cycle was repeated twice to obtain the data in Fig. 9, demonstrating the successful ejection of a single $^{40}Ca^{+}$ ion in each cycle. The ejection voltages listed in Table I turn out to be about 25% higher than the numerical result in Fig. 5(b), just like the case in Fig. 8. The increment in U_B between one ejection cycle and the next was about 40 mV for $V_{in} = 0.3$ V and about 100 mV for $V_{in} = 0.5$ V. As it naturally becomes larger for a higher V_{in}, the use of a deeper axial potential makes each ejection cycle less sensitive to voltage errors.

It is possible to separate a single ion even from a zigzag crystal as experimentally verified in Fig. 10. Starting from a typical zigzag with 12 $^{40}Ca^{+}$ ions, we raised and lowered the Gate-B potential twice to eject the ion at the right end. The experimental conditions, except for N_{in} and U_B,

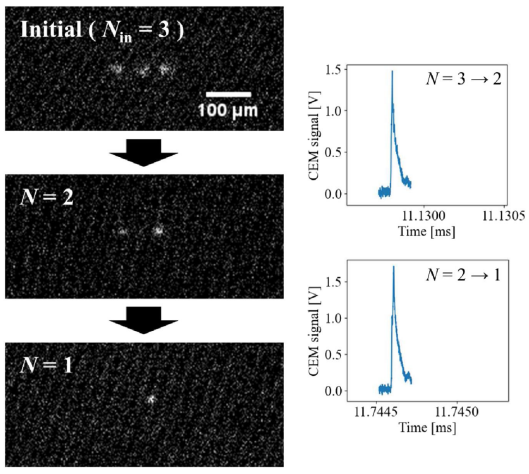


FIG. 9. A sequence of single-ion separation and extraction at $V_{in} = 0.5$ V. The starting crystalline structure is a string consisting of three $^{40}Ca^{+}$ ions ($N_{in} = 3$). The Gate-B voltages at the first and second shots are listed in Table I.

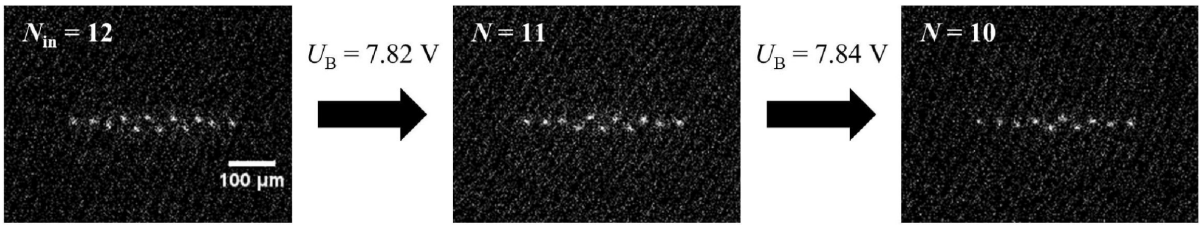


FIG. 10. A sequence of single-ion separation and extraction from a zigzag crystal formed with $V_{in} = 0.3$ V. The voltage V_B on Gate B is raised linearly from 0.3 V to a proper threshold U_B in 10 ms. After keeping the Gate-B potential at U_B for 5 ms, it is reduced to the original value (0.3 V) in 10 ms for LIF measurement. We repeated this cycle twice, choosing slightly different values for U_B.

are identical to those considered in Fig. 8. The upper value of the Gate-B voltage is 7.82 V in the first ejection cycle and 7.84 V in the second; the difference is 20 mV, which is nearly halved compared with the string-based experiment.

We also tried the alternative scheme, i.e., the manipulation of V_A instead of V_B, numerically studied in Sec. III. The idea does work at least in theory, but from a practical point of view, it is relatively difficult to implement. For instance, the Gate voltage must be controlled much more precisely because the usable range of V_A is very narrow; theoretically, it is between 0 V and a certain value well below V_{in}. The numerical result in Fig. 6 suggests that the required accuracy is probably of the order of 0.1 mV or better for $V_{in} = 0.3$ V. We actually observed that more than a few ions escaped from the trap when V_A was lowered only by 10 mV. This decrement is roughly one-fourth of the increment in V_B taken for the experiment in Fig. 8. Moreover, a portion of the ultracold ions was found to remain in the LPT even after we dropped V_A to zero. This is considered as a piece of evidence for the existence of the above-mentioned weak extra potential of unknown origin.

V. CONCLUDING REMARKS

We have experimentally explored the idea of a unique ion source based on a compact Paul ion trap. A non-neutral plasma generated in the new source is already in the ultralow-emittance state before extraction, which enables the creation of extremely narrow nanobeams without the use of any sophisticated collimation and final focusing systems [23]. Since the plasma is Doppler-cooled to near absolute zero temperature and thus Coulomb crystallized in the trap, the ultrahigh-precision orbit control of each individual ion is achievable in principle. We actually succeeded in separating ultracold $^{40}Ca^+$ ions one by one from a Coulomb crystal and ejecting each of them along the LPT axis. In addition to the ion machine-gun scheme (fast extraction) implemented previously [13], the feasibility of a few slow-extraction schemes was tested. It was demonstrated that each single ion can be launched from the LPT at arbitrary timing by manipulating the potential of just one Gate electrode.

Even zigzag-type crystals were found to be usable for our purpose, while all previous experiments had relied on the string configuration [11–14]. A zigzag crystal consists of more ions than any string formed under the same confinement condition. When the number of ions decreases during the ejection process, a zigzag naturally turns to a string. We can, therefore, somewhat ease restrictions on the number of available ions in one ejection sequence, starting with a zigzag crystal rather than a string.

Systematic MD simulations have indicated that the novel ion source developed here makes it possible to irradiate an intended target with a single ion far more precisely than any conventional microbeam schemes [13,21]. The normalized rms emittance of the slowly extracted single-ion beam could be on the order of a femtometer or less, which realizes a spot size of nanometer range on the target. The kinetic energies of all ions from the LPT source are almost exactly equal. A wide variety of ion species are available for the nanobeam because we can cool any ion species sympathetically through Coulomb interaction with laser-coolable ions such as $^{40}Ca^+$ [14,21,24,25].

One of remaining issues is to identify the primary cause of the discrepancy between the MD simulations (Fig. 5) and experimental results (Table I) in the slow-extraction scheme. Another task, even more important, is to establish an advanced nanobeam generation scenario for ion species not directly coolable with laser light. As a first step, we are planning to try separating ultracold $^{14}N^+$ or $^{14}N^{2+}$ ions from two-component Coulomb crystals and accelerate them up to 50 or 100 keV at the Takasaki Institute [15]. We are also preparing for beam-size measurement based on the knife-edge technique [26,27].

The ultrahigh controllability of single-particle motion gives us the possibility of reaching much higher beam energy by an rf accelerator while preserving the string formation and extremely low normalized emittance. For instance, the distances between neighboring ions from the LPT are roughly equal as demonstrated numerically and experimentally (see Fig. 7 and Ref. [13]); the uniformity becomes even better for a string with three ions. It is thus theoretically possible to inject these ions into a linac such that each of them sits close to the stable fixed point of an rf separatrix. In principle, we can even put a single ion near

the center of a particular rf bucket as the injection timing is controllable in the proposed slow-extraction scheme. The chain of ions traveling exactly along the design beam orbit can then be accelerated to very high energy without serious heating due to the synchrotron oscillation excited by the strong rf field.

ACKNOWLEDGMENTS

This work is supported in part by Japan Society for the Promotion of Sciences (JSPS) KAKENHI Grants No. JP24KJ1723 and No. JP25K15770, and by a Japan Science and Technology Agency (JST) Moonshot R&D Grant No. JPMJMS2062.

DATA AVAILABILITY

The data that support the findings of this article are not publicly available upon publication because it is not technically feasible and/or the cost of preparing, depositing, and hosting the data would be prohibitive within the terms of this research project. The data are available from the authors upon reasonable request.

APPENDIX: ION EXTRACTION BY MEANS OF RADIATION PRESSURE

In Sec. III, we numerically considered some practical schemes of ion ejection based on the control of electrode potentials. The idea, probably the most straightforward, was successfully implemented as described in Sec. IV. We here take a brief look at another simple scheme based on the radiation pressure. Laser photons create the dissipative force $\boldsymbol{F}_c$ given by Eq. (1). This force can be employed to push a Coulomb crystal so that the ion at the exit end goes beyond the potential barrier provided by the Gate-A electrode. The strength of $\boldsymbol{F}_c$ is controllable to a certain extent by changing the detuning δ, i.e., the frequency of the cooling laser.

As an example, let us take an initial condition similar to that in Fig. 3. We first form a string crystal of five $^{40}Ca^+$ ions, setting the voltages on the two Gate electrodes at 0.3 V. V_B is then increased to 6.25 V, slightly lower than the final value (6.26 V) chosen in the previous simulation; at this V_B, no ions escape from the LPT. Keeping the Gate-B potential, we change the laser detuning from −60 to −54 MHz in 1 ms. What happens then is exhibited in Fig. 11. Only the rightmost ion has been ejected from the trap slightly after the completion of the detuning sweep.

We now try to launch all five ions consecutively, sweeping the laser frequency over a wider range. For this purpose, the Gate voltages are decreased to 0.01 V to lower the axial potential barrier. V_A and V_B are both fixed at this initial value. In addition, we focus the cooling laser more strongly to reduce the spot size σ from 0.9 to 0.2 mm, which enhances the radiation pressure to the stored ions.

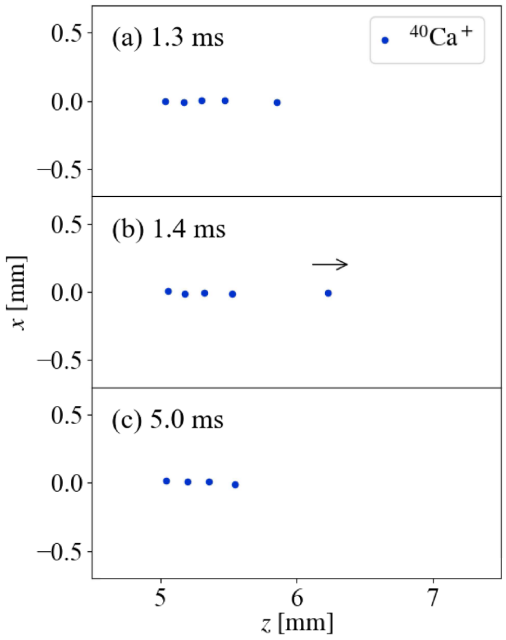


FIG. 11. Single-ion separation from a string Coulomb crystal ($N_{in} = 5$) by means of the radiation pressure generated by the cooling laser. The three panels show the ion distributions at (a) 1.3 ms, (b) 1.4 ms, and (c) 5.0 ms after the change in the laser detuning starts.

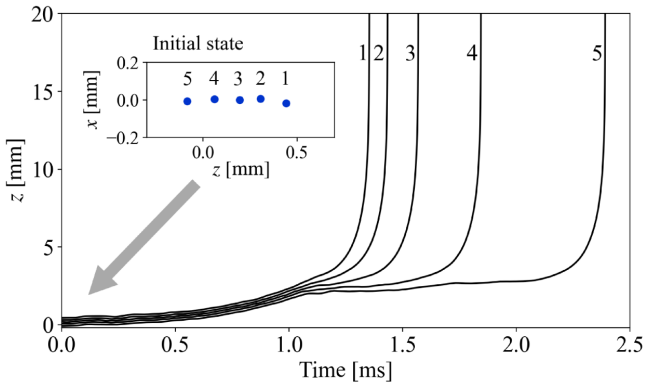


FIG. 12. Axial coordinates of five $^{40}Ca^+$ ions after the start of laser-frequency sweeping. The five ions form a string crystal at $t = 0$ as depicted in the inset. The edge of the LPT is located at $z = 20$ mm. The frequency sweep ends at $t = 1.0$ ms, and afterward, the detuning is maintained at −12 MHz.

The detuning is changed linearly from −240 to −12 MHz in 1 ms and maintained thereafter to keep pushing the ions. The axial positions of the five ions after the start of the detuning sweep are plotted in Fig. 12 indicating the success of our plan; all five ions have been ejected from the LPT at different timings. Note that the ejection begins slightly after the detuning reaches the final value. The time interval from one ejection to the next turns out to be longer as the number of remaining ions decreases.

[1] J. A. van Kan, A. A. Bettiol, and F. Watt, Proton beam writing of three-dimensional nanostructures in hydrogen silsesquioxane, Nano Lett. **6**, 580 (2006).

[2] Y. Iwai, T. Ikeda, T. M. Kojima, Y. Yamazaki, K. Maeshima, N. Imamoto, T. Kobayashi, T. Nebiki, T. Narusawa, and G. P. Pokhil, Ion irradiation in liquid of μm^3 region for cell surgery, Appl. Phys. Lett. **92**, 023509 (2008).

[3] K. M. Prise, G. Schettino, B. Vojnovic, O. Belyakov, and C. Shao, Microbeam studies of the bystander response, J. Radiat. Res. **50**, A1 (2009).

[4] S. Onoda, A. Hasuike, Y. Nabeshima, H. Sasaki, K. Yajima, S.-i. Sato, and T. Ohshima, Enhanced charge collection by single ion strike in AlGaN/GaN HEMTs, IEEE Trans. Nucl. Sci. **60**, 4446 (2013).

[5] D. W. M. Walsh, C. Siebenwirth, C. Greubel, K. Ilicic, J. Reindl, S. Girst, G. Muggiolu, M. Simon, P. Barberet, H. Seznec, H. Zischka, G. Multhoff, T. E. Schmid, and G. Dollinger, Live cell imaging of mitochondria following targeted irradiation in situ reveals rapid and highly localized loss of membrane potential, Sci. Rep. **7**, 46684 (2017).

[6] A. M. Tonigan, D. Ball, G. Vizkelethy, J. Black, D. Black, J. Trippe, E. Bielejec, M. L. Alles, R. Reed, and R. D. Schrimpf, Impact of surface recombination on single-event charge collection in an SOI technology, IEEE Trans. Nucl. Sci. **68**, 305 (2021).

[7] P. K. Ghosh, *Ion Traps* (Oxford Science, Oxford, 1995).

[8] T. W. Hänsch and A. L. Schawlow, Cooling of gases by laser radiation, Opt. Commun. **13**, 68 (1975).

[9] D. J. Wineland and H. Dehmelt, Proposed $10^{14}\delta\nu < \nu$ laser fluorescence spectroscopy on Tl^+ mono-ion oscillator, Bull. Am. Phys. Soc. **20**, 637 (1975).

[10] A. Ogata and H. Okamoto, Extremely low-emittance low-current RFQ with ion-trap injector, in *Quantum Aspect of Beam Physics*, edited by P. Chen (World Scientific, Singapore, 2000), p. 269.

[11] M. Kano, S. Masuda, A. Ogata, K. Okabe, and H. Okamoto, Ultra-low emittance beam generator using Coulomb crystals, J. Phys. Soc. Jpn. **73**, 760 (2004).

[12] W. Schnitzler, N. M. Linke, R. Fickler, J. Meijer, F. Schmidt-Kaler, and K. Singer, Deterministic ultracold ion source targeting the Heisenberg limit, Phys. Rev. Lett. **102**, 070501 (2009).

[13] K. Izawa, K. Ito, H. Higaki, and H. Okamoto, Controlled extraction of ultracold ions from a linear Paul trap for nanobeam production, J. Phys. Soc. Jpn. **79**, 124502 (2010).

[14] K. Groot-Berning, G. Jacob, C. Osterkamp, F. Jelezko, and F. Schmidt-Kaler, Fabrication of $^{15}NV^-$ centers in diamond using a deterministic single ion implanter, New J. Phys. **23**, 063067 (2021).

[15] Y. Yuri, K. Hosaka, N. Miyawaki, Y. Ishii, S. Hosoya, H. Kashiwagi, R. Yamagata, K. Narumi, S. Onoda, K. Muroo, K. Ito, and H. Okamoto, Research and development study on nanobeam formation using laser-cooled ions for high-precision single-ion irradiation, in *Proceedings of 16th International Particle Accelerator Conference (IPAC'25), Taipei, Taiwan* (JACoW, Geneva, Switzerland, 2025), p. 997.

[16] L. W. Swanson, Liquid metal ion sources: Mechanism and applications, Nucl. Instrum. Methods Phys. Res. **218**, 347 (1983).

[17] D. R. Denison, Operating parameters of a quadrupole in a grounded cylindrical housing, J. Vac. Sci. Technol. **8**, 266 (1971).

[18] K. Fukushima and H. Okamoto, Design study of a multipole ion trap for beam physics applications, Plasma Fusion Res. **10**, 1401081 (2015).

[19] A. Rahman and J. P. Schiffer, Structure of a one-component plasma in an external field: A molecular-dynamics study of particle arrangement in a heavy-ion storage ring, Phys. Rev. Lett. **57**, 1133 (1986).

[20] R. W. Hasse and J. P. Schiffer, The structure of cylindrically confined Coulomb lattice, Ann. Phys. (N.Y.) **203**, 419 (1990).

[21] K. Muroo, H. Okamoto, N. Miyawaki, and Y. Yuri, Simulation study of ultrahigh-precision single-ion extraction from a linear Paul trap, Prog. Theor. Exp. Phys. **2023**, 063G01 (2023).

[22] CST Studio Suite, 3D EM simulation and analysis software. Dassault systems, https://www.3ds.com/products-services/simulia/products/cst-studio-suite.

[23] Y. Yuri, N. Miyawaki, K. Hosaka, Y. Ishii, S. Hosoya, H. Kashiwagi, K. Ito, H. Okamoto, and K. Narumi, Investigating ultralow-emittance nanobeam formation using a Coulomb crystal, Prog. Theor. Exp. Phys. **2025**, 023G01 (2025).

[24] D. J. Larson, J. C. Bergquist, J. J. Bollinger, W. M. Itano, and D. J. Wineland, Sympathetic cooling of trapped ions: a laser-cooled two-species nonneutral ion plasma, Phys. Rev. Lett. **57**, 70 (1986).

[25] S. Schiller and C. Lämmerzahl, Molecular dynamics simulation of sympathetic crystallization of molecular ions, Phys. Rev. A **68**, 053406 (2003).

[26] J. A. Arnaud, W. M. Hubbard, G. D. Mandeville, B. de la Clavière, E. A. Franke, and J. M. Franke, Technique for fast measurement of Gaussian laser beam parameter, Appl. Opt. **10**, 2775 (1971).

[27] Y. Ishii, A. Isoya, T. Kojima, and K. Arakawa, Estimation of keV submicron ion beam width using a knife-edge method, Nucl. Instrum. Methods Phys. Res., Sect. B **211**, 415 (2003).